Structure of the R65Q Mutant of Yeast 3-Phosphoglycerate Kinase Complexed with Mg-AMP-PNP and 3-Phospho-D-glycerate[†,‡]

Timothy M. McPhillips,[§] Barbara T. Hsu,[§] Mark A. Sherman,[||] Maria T. Mas,[||] and Douglas C. Rees*[,§]

Division of Chemistry, California Institute of Technology, Pasadena, California 91125, and Beckman Research Institute of the City of Hope, Duarte, California 91010

Received October 19, 1995; Revised Manuscript Received January 26, 1996[⊗]

ABSTRACT: The structure of a ternary complex of the R65Q mutant of yeast 3-phosphoglycerate kinase (PGK) with magnesium 5′-adenylylimidodiphosphate (Mg-AMP-PNP) and 3-phospho-D-glycerate (3-PG) has been determined by X-ray crystallography to 2.4 Å resolution. The structure was solved by single isomorphous replacement, anomalous scattering, and solvent flattening and has been refined to an *R*-factor of 0.185, with rms deviations from ideal bond distance and angles of 0.009 Å and 1.78°, respectively. PGK consists of two domains, with the 3-PG bound to a "basic patch" of residues from the N-terminal domain and the Mg-AMP-PNP interacting with residues from the C-terminal domain. The two ligands are separated by ∼11 Å across the interdomain cleft. The model of the R65Q mutant of yeast PGK is very similar to the structures of PGK isolated from horse, pig, and *Bacillus stearothermophilus* (rms deviations between equivalent α-carbons in the individual domains < 1.0 Å) but exhibits substantial variations with a previously reported yeast structure (rms deviations between equivalent α-carbons in the individual domains of 2.9−3.2 Å). The most significant tertiary structural differences among the yeast R65Q, equine, porcine, and *B. stearothermophilus* PGK structures occur in the relative orientations of the two domains. However, the relationships between the observed conformations of PGK are inconsistent with a "hinge-bending" behavior that would close the interdomain cleft. It is proposed that the available structural and biochemical data on PGK may indicate that the basic patch primarily represents the site of anion activation and not the catalytically active binding site for 3-PG.

PGK catalyzes a key phosphorylation step in the glycolytic pathway. Under physiological conditions, PGK facilitates transfer of the anhydride phosphate of 1,3-bisphospho-D-glycerate (1,3-BPG)[1] to MgADP, yielding 3-phospho-D-glycerate (3-PG) and MgATP (Scopes, 1978a). The instability of the 1,3-BPG substrate makes the reverse reaction more convenient to study under laboratory conditions. Since most mechanistic studies have focused on the MgATP consuming reaction, the glycolytic reactants MgADP and 1,3-BPG are usually referred to as the products of PGK catalysis. Kinetic studies have shown that this catalysis is particularly sensitive to anion concentration (Larsson-Raznikiewicz & Arvidsson, 1971; Schierbeck & Larsson-Raznikiewicz, 1979). The enzyme is activated by low concentrations of anions, including 3-PG, and inhibited by high concentrations of non-substrate anions (Scopes, 1978b).

PGK has a molecular weight of approximately 45 kDa and is monomeric under most conditions (Larsson-Raznikiewicz, 1970). Structural studies of PGK from four species, spanning prokaryotes to mammals, reveal that the single polypeptide chain of PGK folds into two globular domains, the N-domain and the C-domain, of approximately equal size. Approximately 30 of the ∼400 residues make up two polypeptide linkages connecting the two domains. Both domains are involved in substrate binding. Multiple crystallographic studies have demonstrated that nucleotide substrates or analogs bind to the C-domain (Blake & Evans, 1974; Watson et al., 1982; Davies et al., 1994), while a crystallographic study of porcine PGK has confirmed predictions that 3-PG binds to the N-domain in a "basic patch" consisting of arginines 21, 38, 65, 121, and 168 and histidines 62, 167, and 170 (Harlos et al., 1992).

All crystallographic studies agree that the peripheries of the nucleotide binding site and the basic patch are separated by at least 7 Å (Harlos et al., 1992). The large distance between the two apparent substrate binding sites and the similarity between the domain organization of PGK and hexokinase, an enzyme known to exhibit dramatically different open and closed conformations (Bennett & Steitz, 1978), has suggested that PGK also has two very different open and closed conformations (Blake & Rice, 1981). A large "hinge-bending" motion, transforming the enzyme from the open to the closed conformations, could bring the substrates of PGK into proximity before phosphate transfer (Banks et al., 1979), although no crystallographic studies of PGK have revealed the structure of a completely closed conformation. Small-angle X-ray scattering (Pickover et al.,

[†]Supported in part by NIH Grants GM45162 (D.C.R.) and GM37715 (M.T.M.). T.M.M. was supported in part by NIH Predoctoral Training Grant GM07616.

[‡]Coordinates have been deposited in the Brookhaven Protein Data Bank under the file name 1QPG.

* To whom correspondence should be addressed.

[§] California Institute of Technology.

[||] City of Hope.

[⊗] Abstract published in *Advance ACS Abstracts,* March 1, 1996.

[1] Abbreviations: ADP, adenosine diphosphate; AMP-PNP, 5′-adenylylimidodiphosphate; ATP, adenosine triphosphate; 1,3-BPG, 1,3-bisphospho-D-glycerate; CMNP, 2-chloromercuri-4-nitrophenol; HEPES, *N*-2-hydroxyethylpiperazine-*N*′-2-ethanesulfonic acid; PDB, protein data bank; 3-PG, 3-phospho-D-glycerate; PGK, 3-phosphoglycerate kinase; R65Q, mutant of yeast PGK with arginine 65 replaced by glutamine; rms, root mean square; rmsd, root mean square deviation; SIRAS, single isomorphous replacement with anomalous scattering.

0006-2960/96/0435-4118$12.00/0

1979; Timchenko & Tsyuryupa, 1982), fluorescence spectroscopy (Mouawad et al., 1990; Desmadril et al., 1991), NMR (Tanswell et al., 1976; Fairbrother et al., 1990), and other experiments have confirmed that a structural adjustment does occur on 3-PG binding. However, these spectroscopic studies have not clearly described either the nature or the magnitude of this conformational change. In particular, they have not established that a hinge-bending interdomain motion actually occurs in PGK.

Dramatically different open and closed conformations of PGK are necessary to the catalytic mechanism only if the basic patch is the part of the active site that binds the reactive 3-PG during phosphate transfer. If the basic patch is not part of the active site of PGK, then the N-domain need not approach the C-domain as closely. Thus, the observed structural adjustment may interconvert two closely related conformations. This adjustment could subtly modify the true active site to create the catalytically active binding site for 3-PG. In this case, the role of the basic patch could be regulatory, with the binding of 3-PG or other anions to the basic patch altering the equilibrium among different conformations or stabilizing the transition states between them. Evidence has been presented that suggests that 3-PG binds to PGK in multiple sites with both regulatory and catalytic functions (Schierbeck & Larsson-Raznikiewicz, 1979).

The possibility that the basic patch primarily plays a regulatory role is consistent with results of mutagenesis experiments probing the roles of basic patch histidines 62, 167, and 170 and arginines 21, 38, 65, and 168 (Fairbrother et al., 1989a,b; Walker et al., 1989; Sherman et al., 1990, 1991, 1992). These investigations show that although mutagenesis of any of these basic patch residues diminishes the ability of anions to activate PGK, near-total elimination of catalytic activity is observed only for mutations of arginine 38 (Sherman et al., 1992). The failure of the other mutations to dramatically reduce activity suggests that the primary role of the basic patch cannot be catalytic. Indeed, the observation that the mutations in the basic patch primarily impair anion activation indicates the basic patch is involved in anion regulation (Sherman et al, 1990).

To further address the role of basic patch residues in PGK activity and regulation, we have solved the structure of the R65Q mutant of yeast PGK in the presence of 3-PG, Mg^{2+}, and an ATP-analog, AMP-PNP. The most striking consequence of the R65Q substitution is the complete loss of anion activatory behavior, with relatively small effects on catalytic activity. The maximum velocity, V_{max}, of the enzyme is nearly twice that of the wild type enzyme, while the K_m values of the mutant for 3-PG and ATP are increased by factors of 2−6 relative to the wild type values. Thus, the catalytic efficiency of the enzyme is actually reduced by the mutation (Sherman et al., 1991). The crystal structure of this mutant was determined to assess the structural consequences of the R65Q substitution. The high activity of the mutant in the absence of activating anions suggested that the interdomain orientation of the R65Q enzyme might differ significantly from previously reported crystal structures. While differences in the interdomain orientation are observed, they are inconsistent with the changes expected for hinge-bending behavior that would close the interdomain cleft. Rather, the observed variations in the interdomain orientations suggest that the basic patch may primarily serve a regulatory function and that domain-domain motion may create a distinct catalytic binding site for 3-PG.

Table 1: Data Collection and Final Refinement Statistics for Yeast R65Q PGK Complexed with Mg-AMP-PNP and 3-PG

Data Collection Statistics		
	native	CMNP derivative
resolution limit (Å)	2.43	2.75
no. of measured reflns	100 828	52 248
no. of independent reflns	16 281	10 987
data completion (%)	92.4	90.4
R_{sym} (%)	7.65	7.36
Refinement Statistics		
resolution range (Å)	8.0−2.4	
no. of reflns	13 387 (78.3% complete)	
no. of scatterers	3271	
no. of water molecules	82	
WA weight used	3.6×10^5	
rms ΔB values for adjacent atoms	2.0	
crystallographic *R*-factor	0.185	
rms deviations from ideal values		
bonds (Å)	0.009	
angles (deg)	1.78	
dihedrals (deg)	21.7	
impropers (deg)	1.26	

EXPERIMENTAL PROCEDURES

Protein Preparation and Crystallization. The R65Q mutant of yeast 3-phosphoglycerate kinase was isolated as previously described (Sherman et al., 1991). Crystals for X-ray analysis were prepared by the hanging-drop method using Linbro tissue culture plates and silanized glass coverslips. Well solutions consisted of 21% polyethylene glycol-8000, 20 mM magnesium acetate, 0.02% NaN_3, and 50 mM HEPES at pH 7.5. The hanging drops were prepared by mixing the well solution with an equal volume of a protein/substrate solution containing 18 mg/mL of R65Q PGK; 10 mM 5′-adenylylimidodiphosphate, tetralithium salt (AMP-PNP); and 10 mM D-(−)-3-phosphoglycerate, disodium salt (3-PG). The presence of both substrates was required for crystallization. Drops 10−20 μL in volume were equilibrated against well solution at 4 °C. Microcrystals grown over a period of 2 weeks were transferred to fresh drops that had been pre-equilibrated against well solution for 2 days. A reiteration of this macroseeding procedure resulted in the growth of crystals with dimensions as large as $2.0 \times 0.5 \times 0.3$ mm^3. The crystals were determined to be of the monoclinic space group *C*2, with unit cell parameters $a = 96.0$ Å, $b = 70.1$ Å, $c = 82.3$ Å, $\beta = 122.2°$, and $Z = 4$.

Data Collection. X-ray diffraction data were collected at room temperature on crystals mounted in quartz capillaries. X-rays were generated using a Siemens rotating anode with a Cu target operating at 4500 W (50 kV × 90 mA). A graphite monochromator was used to select the Cu Kα wavelength of 1.5418 Å. X-ray diffraction measurements were made using a Siemens X-1000 multiwire area detector. All data were indexed, integrated, and scaled using the program XENGEN (Howard et al., 1987). The native and derivative data sets were collected on one crystal each. Table 1 provides data collection statistics for both data sets.

Molecular Replacement Attempt. Phasing by molecular replacement was attempted using X-PLOR (Brünger, 1992). The search model used was the yeast PGK coordinate set 3PGK (Watson et. al., 1982) from the Brookhaven protein

data base (Bernstein et al., 1977). Top solutions from the rotation function were refined against the Patterson-correlation function in X-PLOR. In order to account for possible differences in the relative orientations of the domains, the model used for PC-refinement was broken into three rigid bodies corresponding to the N-domain, the C-domain, and the interdomain junction. Although a translation search using the best result from PC-refinement gave an unambiguous solution, maps calculated from this solution were poor.

SIRAS Phasing and Solvent Flattening. A single heavy-atom derivative data set (see Table 1) was collected from a crystal soaked in a solution of 2-chloromercuri-4-nitrophenol (CMNP) and used for phasing. A single Hg(II) site was located from a difference-Patterson map. The program PHASES (Furey & Swaminathan, 1990) was then used to refine the heavy-atom parameters, resulting in fractional cell coordinates of $x = 0.1164$ and $z = 0.0411$, and an isotropic *B*-factor of 34.01 Å^2. Phases were calculated from both isomorphous difference and anomalous scattering effects to 2.90 Å resolution. The overall phasing power from single isomorphous replacement effects was 2.72 for 9520 reflections. For anomalous scattering, the overall phasing power was 2.47 for 8697 reflections. The overall figure of merit for the 9520 reflections phased was 0.665 at this stage.

Maps calculated using the SIRAS phases alone were not clear enough to build a model. Comparison of the Hg(II) site in the derivative with the molecular replacement solution indicated that the metal atom was near the only cysteine residue (C97) in the model. Combination of the SIRAS phases with the molecular replacement model phases did not improve the quality of the maps, however. In the end, no phase information from the molecular replacement solution was used in solving the structure.

The SIRAS phases were substantially improved by solvent flattening using PHASES. A solvent fraction of 30% and a sphere radius of 8 Å were used for calculating the Wang solvent masks. A total of three successive solvent masks were used over the course of 28 cycles of solvent flattening. No phase extension was performed. The *R*-factor between observed structure factors and those calculated from the final, solvent-flattened map was 18.5%. The final overall figure of merit for the 9520 phased reflections was 0.863. An electron density map calculated using the solvent-flattened phases was interpretable in most of the unflattened region.

Model Building and Refinement. All model building was performed with TOM/FRODO (Jones, 1985) modified to run on a Silicon Graphics workstation. The AMP-PNP molecule and nearly 80% of the peptide chain were built into the solvent-flattened map. Refining the initial coordinates with the TNT package (Tronrud et al., 1987) yielded an *R*-factor of 0.390 to 2.9 Å resolution. A phase-combined map was calculated, and model building resumed. Four cycles of model building, TNT refinement, and phase combination revealed the remaining residues and reduced the *R*-factor to 0.251 at 2.9 Å resolution.

No solvent molecules were added until further model building followed by X-PLOR (Brünger, 1992) refinement had reduced the *R*-factor to 19.8% at 2.4 Å resolution, with rms bond and angle deviations of 0.017 Å and 2.1° from ideality. Water molecules were added where $F_o - F_c$ positive difference peaks of at least 3.0σ height occurred in chemically reasonable positions. Occupancies for all waters were fixed at 1.0, and the *B*-factors were left unrestrained during refinement. Electron density corresponding in shape and size to a 3-PG molecule was observed in maps calculated in the final stages of model building and refinement. Refinement of a 3-PG molecule modeled in this density resulted in high *B*-factors for the 3-PG atoms, indicating partial occupancy of the site or disordering of the molecule. The occupancy of the 3-PG molecule was set to 0.50 for the final refinements which yielded an average *B*-factor of 62 Å^2 for the 3-PG atoms, but clear electron density for the substrate.

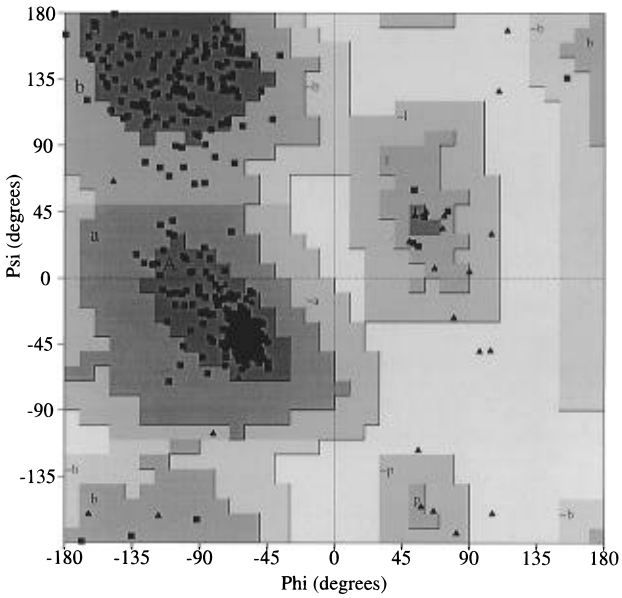

FIGURE 1: Ramachandran diagram for the final refined coordinates. Glycines are shown as triangles, and non-glycine residues are shown as squares. Drawn with PROCHECK (Laskowski et al., 1993).

The final *R*-factor after refinement is 0.185, calculated using all positive structure factors in the data set above 8.0 Å resolution, without application of a σ cutoff or bulk solvent correction. The restraint weight used was that calculated by the CHECK routine of X-PLOR yielding rms bond and angle deviations from ideality of 0.009 Å and 1.78°, respectively. The Ramachandran plot from PROCHECK (Laskowski et al., 1993) in Figure 1 shows that over 88% of the non-glycine, non-proline residues are found in the most favored regions, with no residues in disallowed regions. Analysis of side chain geometry by $\chi_1 - \chi_2$ plots does not indicate any unfavorable conformations.

Seven short segments of the chain, containing residues 29−32, 132−136, 287−297, 301−307, 340−348, 360−364, and 377−385, appear to be either somewhat disordered or thermally mobile about the average, modeled position. Ambiguities in these sections of the structure were resolved by best fit to the available density and use of geometric constraints imposed by distinct density in adjoining regions. Additionally, negligible density was observed for the side chains of 13 non-glycine, non-alanine residues. The occupancies of the side chain atoms beyond C_β in these residues were fixed at zero for all structure factor calculations. Occupancies of atoms of residue 415 were similarly treated because they lacked density. Overall, the average *B*-factor in the N-domain, 31 Å^2, is lower than in the C-domain, 39 Å^2, reflecting a clearer electron density map of the N-domain than of the C-domain. The final model consists of all 415 protein residues, the AMP-PNP and 3-PG molecules, a single Mg^{2+} ion, and 82 water molecules. Coordinates have been

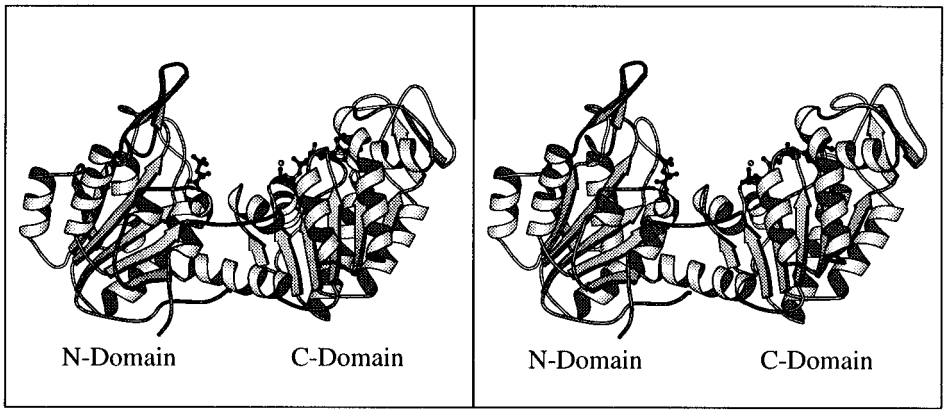

FIGURE 2: Stereoview of the overall structure of yeast R65Q PGK. The ball-and-stick structures represent the nucleotide substrate analog Mg-AMP-PNP bound to the C-domain and 3-PG bound to the basic patch of the N-domain. Drawn with MOLSCRIPT (Kraulis, 1991).

Table 2: Constituent Residues of Secondary Elements in Yeast Phosphoglycerate Kinase[a]

N-domain				C-domain			
β-strands		α-helices		β-Strands		α-helices	
A	16−23	1a	36−41	G	205−210	8	217−227
		1b	42−52	H	229−234	9	236−246
B	56−63	2	76−88			10	257−273
C	89−94	3	100−108	I	275−280		
D	113−118			o	282−286		
m	129−132			p	294−299	11	315−327
n	135−139	4	141−154	J	330−334	12	346−362
E	157−162	5	163−167	K	365−369	13	371−380
		6	171−174	L	388−390	14	394−401
F	180−184	7	185−199			15	406−410

[a] Parallel β-strands in each domain are labeled sequentially by uppercase letters. Antiparallel β-strands are labeled with lowercase letters. Helices are numbered in sequential order. Helix 1 is broken by proline 44 into two sections labeled 1a and 1b.

deposited in the Brookhaven Protein Data Bank (Bernstein et al., 1977).

Analysis of Domain Orientation. The relative orientation of the N-domain and C-domain in the yeast R65Q structure was compared to orientations observed in structures of PGK from horse (Blake & Rice, 1981), pig (Harlos et al., 1992), and *Bacillus stearothermophilis* (Davies et al., 1994). First, the four structures were superimposed (Kabsch, 1976) using only atoms from the N-domains in the superposition algorithm. This overlaid the N-domains on each other but left the C-domains askew. Next, the C-domain of each structure was transformed to best superimpose on the C-domains of the other structures. Each of these transformations was then resolved into a rotation about the center of mass of the moving C-domain and a translation of it to superimpose it on the stationary C-domain.

RESULTS

Description of the Structure. As in previously described PGK structures, the single polypeptide chain of yeast R65Q folds into two domains, the N-domain and C-domain, consisting of residues 1−184 and 200−393, respectively. The remaining residues of the 415 amino acids in the sequence constitute the interdomain linkage. Each domain folds as an α/β, twisted open-sheet structure composed of a single sheet of six parallel β-strands sandwiched between four long α-helices, two to a side. In addition, each domain has a pair of antiparallel β-strands located above the C-termini of the parallel β-strands. Both pairs of antiparallel β-strands end in solvent-exposed loops. A ribbon diagram of the structure is given in Figure 2.

The secondary structural elements are listed in Table 2, labeled according to the equine PGK nomenclature (Banks et al., 1979). β-Strands A−F form the core of the N-domain in the order CDBAEF (counting toward the C-domain). This sheet is shielded by helices 1 and 2 on one side and helices 3 and 4 on the other. The core of the C-domain is made up of β-strands G−L in the order IHGJKL (counting toward the N-domain). Helices 8 and 10 shield one side of this sheet, while helices 11 and 12 border the opposite face. In both domains, the final β-strand is the one nearest the opposite domain. Each precedes a helix that crosses the interdomain space: helix 7 follows strand F, and helix 14 follows strand L.

There are five α-helices in addition to the helices previously described. The short helix 15 follows helix 14 and associates with the N-domain next to the very short helical element 6. Helix 5 consists of a single turn preceding helix 6 and forms an integral part of the interdomain junction. Elements 9 and 13 are helices of medium length in the C-domain perpendicular to the direction of the core strands. Helix 9 is on a skew line parallel to the β-sheet. The N-terminus of this helix forms part of the hydrophobic pocket in which the nucleotide binds. Helix 13 is normal to the β-sheet, with the N-terminus near the triphosphate group of the nucleotide.

Nucleotide Binding Site and Conformation of AMP-PNP. The residues following the C-termini of five of the core β-strands in the C-domain form a hydrophobic pocket on the surface of the protein facing the opposite domain. The pocket is bordered by residues 210−220, 235−239, 334−341, 370−373, and 393−397, following β-strands G, H, J,

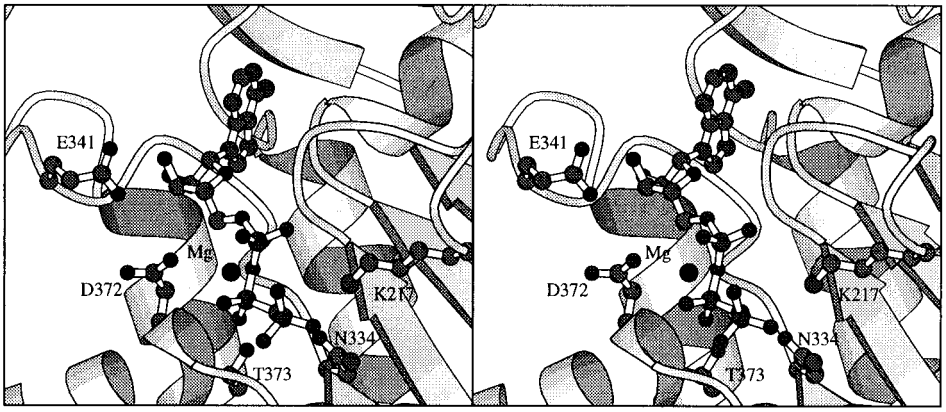

FIGURE 3: Stereoview of Mg-AMP-PNP bound to the nucleotide binding site on the C-domain of yeast R65Q PGK. Side chains that interact with the nucleotide are labeled. Drawn with MOLSCRIPT (Kraulis, 1991).

Table 3: Hydrogen Bond Distances Between Mg-AMP-PNP and Yeast R65Q PGK

atom from nucleotide	atom from protein/solvent	distance (Å)	atom from nucleotide	atom from protein/solvent	distance (Å)
N6	NGly 236	3.5	O1B	NGly 371	3.1
	OGly 310	3.4		NAsp 372	2.7
	O Wat 545	2.6			
			O1A	O Wat 541	2.9
N7	O Wat 545	3.4			
			O2B	OG1Thr 373	2.6
O2′	OE1Glu 341	3.4		NGly 371	3.6
	OE2Glu 341	2.9		NAsp 372	3.3
	OGly 338	3.1		NThr 373	2.9
	NPhe 340	3.4			
			O2G	NGly 371	2.8
O3′	OE1Glu 341	2.9			
	OE2Glu 341	3.1	O3G	ND2Asn 334	3.4
O4′	NAla 212	3.8	N3B	OD1Asn 334	2.8

K, and L, respectively. Residues 253, 254, 310, and 311 also contribute to the surface of the pocket. A molecule of AMP-PNP is bound in this pocket, stretched out along the top of the sheet. The nucleotide is oriented with the adenine ring distal to the N-domain and the triphosphate moiety adjacent to the interdomain cleft. Figure 3 shows the nucleotide and the residues that directly interact with it. Pertinent hydrogen bond distance information is given in Table 3.

The conformation of the nucleotide is currently modeled with a C2′-*endo* ribose group *anti* to the adenine ring. The Mg^{2+} ion is coordinated by a single, nonbridging oxygen atom from each phosphate group. The phosphate oxygen ligands occupy *cis* coordination sites of a distorted octahedron. This α,β,γ-tridentate coordination of a divalent metal ion by a triphosphate group has been observed previously in the crystal structures of the magnesium and manganese complexes of ATP (Cini et al., 1984; Sabat et al., 1985). The magnesium ion is also coordinated by a single carboxylate oxygen of Asp 372, with the carboxylate oxygen *trans* to the γ-phosphate oxygen. Water molecules presumably occupy the remaining two octahedral coordination sites of the metal ion but are not visible in the electron density map.

Basic Patch and 3-PG Binding Site. Just as the residues following five of the core β-strands of the C-domain form the nucleotide binding pocket, the residues following four of the core β-strands of the N-domain form the anion binding pocket, or basic patch. Residues 21−25, 62−67, and 121 are on turns following β-strands A, B, and D, respectively, and form one side of the pocket. Residues 162−171 follow strand E, include helix 5, and make up the opposite face of the pocket. Charged and polar side chains in the basic patch are contributed by arginines 21, 38, 121, and 168; histidines 62, 167, and 170; asparagines 25 and 67; glutamine 65; threonine 165; and aspartate 23.

Electron density for a 3-PG molecule occupies the center of the basic patch. Refinement of a 3-PG model against the crystallographic data resulted in high *B*-factors for the 3-PG atoms. Setting the occupancy of the 3-PG atoms to 0.5 resulted in *B*-factors between 50 and 75 Å^2 for the 3-PG atoms, with atoms at the carboxyl end of the molecule having the lowest *B*-factor, and the phosphate atoms having the highest. Although the density is well defined (see Figure 4), this behavior indicates that the 3-PG is either present in low occupancy or disordered around the modeled position. The model of 3-PG that best fits the observed density indicates that the 3-PG carboxyl group interacts with the side chains of D23, N25, R38, and H62 (Figure 5). The 3-PG hydroxyl group interacts favorably with side chains of N25 and R38, and the 3-PG phosphate binds to the side chains of H62 and R121. The shape of the electron density (see Figure 4), however, indicates that a significant population of 3-PG may occupy the basic patch in an orientation opposite of that modeled, with the phosphate and carboxyl groups reversed.

Comparison with Other PGK Structures. Comparison of the present model of yeast PGK with PDB (Bernstein et al., 1977) entry 3PGK (Watson et al., 1982) revealed significant differences. While the overall topology of the two yeast structures is nearly the same, least-squares superposition of the α-carbon positions in the two structures yielded an rms deviation of 3.4 Å. Superposition of the N- and C-domains separately provided comparable values (2.9 Å for residues 1−185 and 3.2 Å for residues 199−393), indicating that the differences between the two structures reflect differences within the domains, and not in the relative orientation of the domains. In particular, the β-strands in the core of the C-domain in our model are much less curved along their lengths than in 3PGK, and this behavior gives rise to most of the other differences in the C-domain. According to the header of the PDB file, the 3PGK coordinates were obtained by "normalizing" a model built into an experimental electron density map. Consequently, it is likely that many of the discrepancies between the R65Q and 3PGK structures

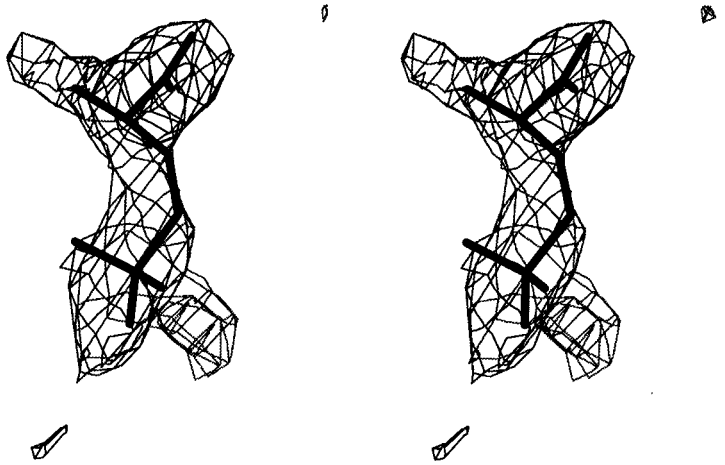

FIGURE 4: Stereoview of omit−refine difference density for 3-PG bound to the basic patch on the N-domain of yeast R65Q PGK. The contour level shown is 2.0σ. 3-PG coordinates shown are those resulting from refinement before omission. The extra density adjacent to the phosphate group may arise from a population of 3-PG molecules bound with the phosphate and carboxyl groups reversed.

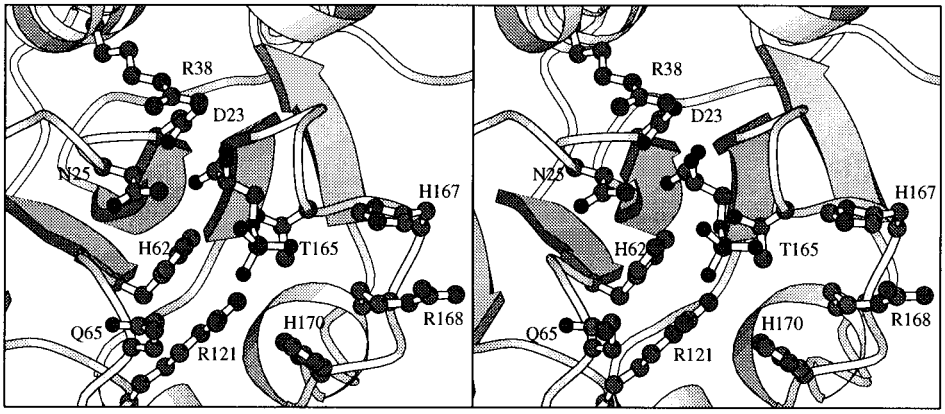

FIGURE 5: Stereoview of 3-PG bound to the basic patch on the N-domain of yeast R65Q PGK. Side chains that interact with the substrate are labeled. Drawn with MOLSCRIPT (Kraulis, 1991).

originate from the unrefined state of the 3PGK model, and do not reflect genuine biochemical differences between the structures.

In contrast, the R65Q yeast structure is very similar to PGK structures from three other species: horse (Blake & Rice, 1981), pig (Harlos et al., 1992), and *B. stearothermophilus* (Davies et al., 1994). Table 4 indicates the results of least-squares superpositions of the R65Q PGK model onto PGK structures from these species. Calculations based on single domains resulted in each case in an rms deviation of less than 1 Å, with an average rmsd of 0.87 Å for the six single domain comparisons. The three rms deviations resulting from whole-molecule comparisons are also significantly lower (the largest is 2.0 Å) than the whole-molecule RMSD value for 3PGK (3.4 Å).

Chothia and Lesk (1986) have noted that the rmsd between two homologous structures can be estimated to within ~20% using the equation

$$\Delta = 0.40e^{1.87H}$$

where H is the fraction of the sequence different between the two homologous structures and Δ is the predicted rms deviation in main chain atom positions in angstroms (Chothia & Lesk, 1986). Estimates for the deviations between yeast PGK and PGK from pig, horse, and bacteria are included in Table 4. The observed rmsd values differ no more than ±22% from the predicted values for each single-domain superposition. The average deviation of the observed rmsd values is only 4% higher than the estimates. Thus, the structure of each domain of yeast R65Q PGK appears to be equivalent to that observed in each of the other species.

Table 4: Results of Superimposing Yeast R65Q PGK Coordinates on PGK Structures from Three Other Species[a]

	N-domain	C-domain	both
B. stearothermophilus			
no. of α-carbons used	156	186	372
sequence identity	0.51	0.54	0.53
predicted rmsd	1.00	0.95	0.96
observed rmsd	0.78	0.91	1.22
horse			
no. of α-carbons used	173	185	390
sequence identity	0.62	0.67	0.65
predicted rmsd	0.81	0.74	0.77
observed rmsd	0.93	0.89	1.46
pig			
no. of α-carbons used	173	200	405
sequence identity	0.62	0.66	0.65
predicted rmsd	0.81	0.76	0.77
observed rmsd	0.94	0.78	2.02

[a] Superposition was performed for residues in the N-domain, the C-domain, and the entire molecule. α-Carbons corresponding to yeast residues 1−4 (N-terminal segment), 186−198 (helix 7), and 400−415 (C-terminal segment) were included in the whole molecule superpositions only. Residues in antiparallel β-strands m and n, and residues near insertions or deletions were not included in any of the calculations. Residues in helix 13 were not used in calculations involving horse PGK. The rms deviations are in angstroms.

Table 5: Rotational and Translational Components of Coordinate Transformations Relating the C-Domain Orientations in PGK from Four Different Crystal Structures[a]

	final orientations		
starting orientations	pig	horse	bacteria
yeast R65Q	$\phi = -91°$, $\psi = 113°$, $\kappa = 15°$ $\Delta x = 4.0$, $\Delta y = -2.8$, $\Delta z = -0.1$	$\phi = -92°$, $\psi = 89°$, $\kappa = 9°$ $\Delta x = 0.6$, $\Delta y = 0.3$, $\Delta z = 0.9$	$\phi = -72°$, $\psi = 89°$, $\kappa = 7°$ $\Delta x = 0.9$, $\Delta y = 0.2$, $\Delta z = -0.2$
bacteria	$\phi = -109°$, $\psi = 128°$, $\kappa = 9°$ $\Delta x = 3.2$, $\Delta y = -2.9$, $\Delta z = 0.0$	$\phi = -154°$,$\psi = 77°$, $\kappa = 3°$ $\Delta x = -0.3$, $\Delta y = 0.2$, $\Delta z = 1.1$	
horse	$\phi = -84°$, $\psi = 138°$, $\kappa = 8°$ $\Delta x = 3.5$, $\Delta y = -3.2$, $\Delta z = -1.1$		

[a] Each transformation superimposes a C-domain in a starting orientation on a C-domain in a final orientation. Rotations are represented as spherical polar angles measured from the *y*-axis. Translations are represented as components along the coordinate axes of an orthogonal reference frame in angstroms.

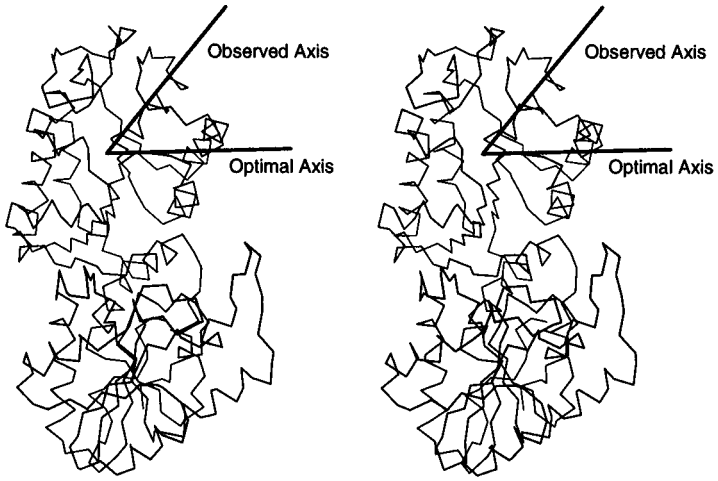

FIGURE 6: Direction of the observed, average interdomain rotation axis in PGK and comparison with the optimal rotation axis for domain closure by hinge-bending.

In contrast to the situation for individual domains, however, the observed rms deviations resulting from whole-molecule comparisons are larger than predicted, with bacterial PGK having the smallest deviation and porcine PGK having the largest deviation from yeast PGK. Since the individual domains superimpose well, differences in the relative orientation of the domains must be responsible for the larger sizes of the whole-molecule RMS deviations. Larger deviations indicate correspondingly greater differences in relative orientation. Thus, the rmsd values suggest that the relative domain orientation of the yeast R65Q structure is most like that of *B. stearothermophilus* PGK and least like that of porcine PGK.

Analysis of the relative orientation of the domains of PGK in the yeast R65Q, equine, porcine, and bacterial PGK structures supports this conclusion. Table 5 lists the rigid-body coordinate transformations required to superimpose the C-domain of each of these structures on the C-domains of the other structures, starting from molecules with superimposed N-domains. The rotational relationships between the C-domains of the four structures may be summarized as

$$\text{yeast (R65Q)} \xrightarrow{\substack{8° \text{ rotation,} \\ \text{axis 1}}} \text{horse, bacteria} \xrightarrow{\substack{8° \text{ rotation,} \\ \text{axis 2}}} \text{pig}$$

The porcine and yeast PGK structures represent the most divergent conformations of this set of structures, being related by a 15° rotation (see Table 5). The horse and bacterial PGK structures represent an intermediate conformation between the pig and yeast R65Q PGK structures. Since the relative positions of the two domains are similar in the equine and bacterial structures, transformations involving the equine and bacterial C-domains are also similar. The average rotation axis relating all three conformations of PGK is shown in Figure 6.

DISCUSSION

The chief consequence of the R65Q mutation to PGK is the loss of anion-activatory behavior. The activity of the enzyme is relatively high in the absence of anions and does not increase in the presence of anions. Comparing the R65Q form of yeast PGK to equine, porcine, and bacterial forms of PGK, all of which contain an arginine at this site, indicates that the mutation does not change the tertiary structure significantly. Instead, the mutation may change the catalytic properties of PGK by altering the dynamics of the enzyme or by shifting the equilibria among various conformations of PGK. Such an effect is consistent with the kinetics of other mutations of yeast PGK. Mutations outside the catalytic and regulatory sites, but near the interdomain region, can have a much greater effect on anion-regulatory behavior than on catalytic activity (Mas et al., 1988). In particular, the S412C, S412P, S412L, and E404C mutants of yeast PGK show kinetic behavior similar to that of the R65Q mutation, despite being far removed from substrate binding sites (H.-H. Chen and M. T. Mas, unpublished results). Like the R65Q mutation, such mutations may emulate anion-activation by perturbing the interdomain region slightly and, thus, altering the distribution of conformations of PGK.

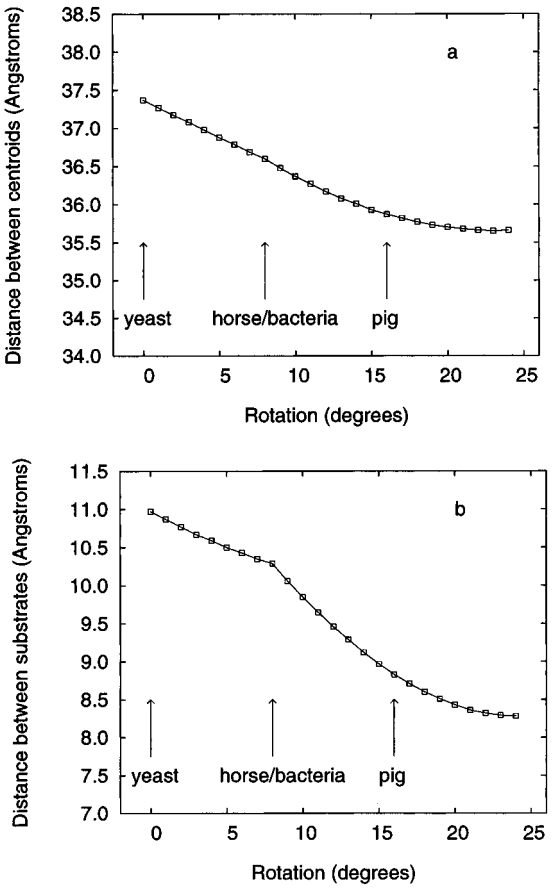

FIGURE 7: (a) Distance between the centroids of the N- and C-domains of the transformed coordinates of yeast R65Q PGK as a function of rotation angle. (b) Distance between substrates in the transformed coordinates of yeast R65Q PGK as a function of rotation angle.

The crystal structures of yeast, equine, porcine, and bacterial PGK may represent samples of PGK conformations in solution. As stated earlier, comparing the yeast, equine, porcine, and bacterial forms of PGK shows that, within the domains, all four species have essentially the same structure. The small structural variations observed within the domains are consistent with predicted variations among homologous proteins with different sequences. In contrast, substantial variations are observed in the relative orientations of the N- and C-domains of the available PGK structures. While sequence differences complicate the analysis, the observed variations in domain positions may reflect different natural conformations of PGK selected by ligand and solution conditions. Assuming that the crystallographically observed orientations of the PGK domains represent a few possible orientations out of a continuous range of motion, it is possible to generate a series of PGK structures that encompass the observed orientations by applying the transformations of Table 5 to the yeast R65Q structure. This type of analysis has been described recently by Vonrhein et al. (1995) to characterize domain motions in adenylate kinase.

The resulting generated structures were examined to determine whether these transformations can close the domains or decrease the distance between the basic patch and the nucleotide binding site. The distance between the centroids of the two domains and the distance between 3-PG and AMP-PNP in the generated structures are plotted in Figure 7. The distance between the domain centroids decreases only 1.7 Å over 24° of rotation, while the minimum distance between the carboxylate oxygen of 3-PG and the phosphate of the nucleotide is 8.3 Å over the same range of motion. Continuing the rotations and translations beyond those observed crystallographically does not result in either the domains or the substrates moving significantly closer.

This analysis further indicates that the rotations and translations relating the observed conformations of PGK differ significantly from those optimal for domain closure or hinge-bending. The optimal translation vector for domain closure would be directed along the vector between the centroids of the two domains. Similarly, the optimal translation vector for joining the basic patch and nucleotide binding site would be along the translation vector between the 3-PG and AMP-PNP molecules. The optimal rotation axis for both operations would be one normal to both the intercentroid and intersubstrate vectors. Table 6 compares these optimal rotation and translation axes with those relating the crystallographically observed orientations of the domains, and Figure 6 shows the direction of the optimal rotation axis along with that of the observed average rotation axis. In the first 8° of rotation/translation, the observed translation axis is fairly close to the optimal translations for domain closure. However, the actual translation along this axis is only 1.0 Å, and the observed rotation axis deviates more than 70° from the optimal axis. In the final 8° of rotation/translation, the rotation axis is less than 30° from the optimal axis, but the translation vector is nearly 80° away from the intercentroid vector, and nearly 70° away from the intersubstrate vector. Thus, the 4.6 Å translation along this axis results in only a 1 Å decrease in the distance between the centroids and less than a 2 Å decrease in the distance between the substrates. Consequently, the observed structures are more nearly interconverted by a "twisting" type motion around the interdomain vector than by a hinge-bending type change.

Although the domain motions relating the observed conformations of PGK do not bring the two domains together, the conformation of the polypeptide chain in the interdomain junction does change. To keep the two domains connected over the range of domain motion, the segments of the polypeptide chain bridging the two domains must adjust to compensate for the motion. Helix 7 either rotates about an axis perpendicular to its length or bends significantly to accommodate the changing orientation of the domains. Similarly, helix 14 translates in a piston-like fashion along its axis to keep the domains connected. Comparison of the yeast and porcine structures illustrates the motions of the interdomain helices. Helix 7 is nearly straight in the porcine structure but is clearly bent in the yeast structure. Helix 14 in the porcine structure is shifted 1.5 Å toward its N-terminus with respect to the helix in the yeast structure. Interestingly, the short helix 5 which forms one side of the basic patch in the N-domain is in contact with helix 14 in both structures. Consequently, it too is shifted toward its N-terminus, altering the geometry of the basic patch. This explains one difference in the way 3-PG binds to the basic patches of the pig and yeast structures. Shifting helix 5 in the pig structure allows R168 at the C-terminus of helix 5 to bind the phosphate group of the 3-PG molecule in the basic patch. In contrast, R168 is too far away from the 3-PG to bind it in the yeast structure. This observation suggests that the affinity of the basic patch for 3-PG varies with the orientation of the two domains.

Table 6: Comparison of the Rotation and Translation Axes Optimal for Domain Closure with the Observed Rotations and Translations[a]

	optimal direction	observed direction	angular deviation
first 8° of rotation			
rotation axis	$\phi = -109°, \psi = 160°$	$\phi = -82°, \psi = 89°$	73°
translation vectors			
intercentroid	$\phi = 129°, \psi = 101°$	$\phi = 154°, \psi = 105°$	26°
intersubstrate	$\phi = 138°, \psi = 98°$		22°
last 8° of rotation			
rotation axis	$\phi = -131°, \psi = 132°$	$\phi = -97°, \psi = 133°$	27°
translation axes			
intercentroid	$\phi = 127°, \psi = 102°$	$\phi = 170°, \psi = 48°$	77°
intersubstrate	$\phi = 135°, \psi = 94°$		69°
full rotation			
rotation axis	$\phi = -109°, \psi = 160°$	$\phi = -91°, \psi = 113°$	48°
translation axes			
intercentroid	$\phi = 129°, \psi = 101°$	$\phi = 179°, \psi = 55°$	67°
intersubstrate	$\phi = 138°, \psi = 98°$		59°

[a] The optimal translation axis for domain closure is defined as a vector directed from the centroid of the C-domain toward the centroid of the N-domain. The optimal translation axis for joining the basic patch with the nucleotide binding pocket is defined as the vector from the γ-phosphate of the nucleotide on the C-domain to the carboxyl group of 3-PG on the N-domain. The optimal rotation axis is defined as a vector normal to the two optimal translation vectors.

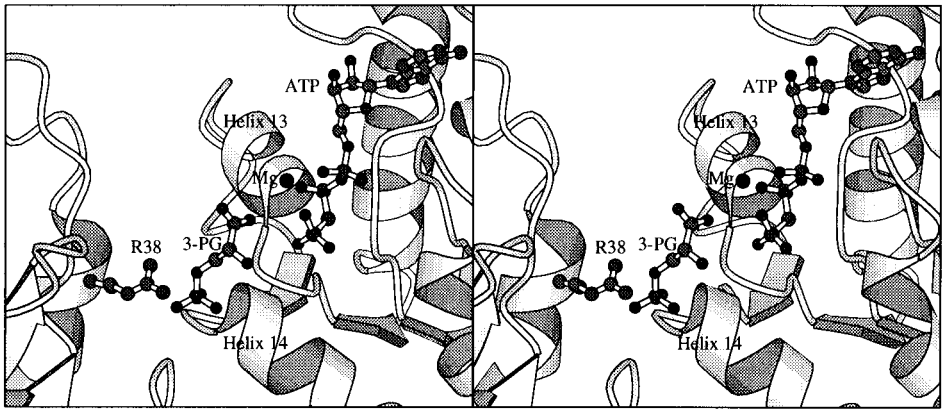

FIGURE 8: Result of modeling 3-PG into the porcine PGK coordinates adjacent to the N-terminus of helix 14. The protein structure shown, including the conformation of R38, is based on the refined coordinates of porcine PGK. The nucleotide coordinates result from superpositioning the R65Q yeast PGK coordinates on the C-domain of the porcine coordinates and transferring the Mg-AMP-PNP coordinates to the porcine model. The 3-PG molecule was positioned by hand. Drawn with MOLSCRIPT (Kraulis, 1991).

Conversely, the observation might imply that the most favored orientation of the two domains depends on whether 3-PG is bound in the basic patch. This agrees with solution studies that indicate that conformational changes are associated with 3-PG binding to PGK (Pickover et al., 1979; Timchenko & Tsyuryupa, 1982).

If, as the crystallographic evidence suggests, the interdomain motion in PGK is insufficient to position the two substrates close enough for phosphate transfer, then another mechanism must be operative. Observing the changes as the interdomain helices move from the yeast to the other PGK structures suggests one possible mechanism. As a result of the changes described above, a potential binding site for the phosphate group of 3-PG appears at the N-terminal end of helix 14. Three sequential glycines, residues 392−394, are positioned at this location, and they form a structure similar to the P-loop, a phosphate binding structural element found in many nucleotide binding proteins (Schulz, 1992). The side chain of R38, the only basic patch residue currently believed essential for catalysis, is near the porcine counterpart of yeast G394 (minimum distance = 4.6 Å). The distance between R38 and G394 varies among the different structures and is 6.9 Å in yeast PGK. This suggests that interdomain motion may help create a catalytic binding site for 3-PG with the Gly-Gly-Gly sequence at the N-terminal region of helix 14 and the side chain of R38. This position has already been suggested to be a possible binding site for 3-PG (Watson, 1982). The 3-PG may not bind to this site in the present crystal structure because either lattice packing interactions or solution conditions selected a conformation of PGK without the proposed binding site. Modeling 3-PG into this proposed site in the pig structure, with the Mg-AMP-PNP molecule positioned as in the yeast R65Q structure, allows the carboxyl group of 3-PG to coordinate the Mg^{2+} ion (see Figure 8). Coordination of the metal ion by 3-PG in this fashion could be the first step in the phosphoryl transfer reaction. Thus, the combination of the nucleotide binding site and the potential 3-PG binding site at the N-terminus of helix 14 may represent the true active site of PGK, while the basic patch serves as an anion-binding region that modulates the interconversion among different interdomain orientations.

ACKNOWLEDGMENT

The authors thank Dr. Colin F. Blake (Oxford) for providing the unpublished atomic coordinates (porcine PGK, 2.0 Å resolution; equine PGK, 2.5 Å resolution) used in the comparative studies. M.T.M. thanks Dr. J. Kraut (UCSD) and members of his laboratory for hospitality and training

in protein crystallization. T.M.M. thanks Ruth Ann Bertsch for invaluable discussions and editing of the manuscript.

REFERENCES

Banks, R. D., Blake, C. C. F, Evans, P. R., Haser, R., Rice, D. W., Hardy, G. W., Merrett, M., & Phillips, A. W. (1979) *Nature 279*, 773−777.

Bennett, W. S., Jr., & Steitz, T. A. (1978) *Proc. Natl. Acad. Sci. U.S.A. 75*, 4848−4852.

Bernstein, F. C., & Tasumi, M. (1977) *J. Appl. Crystallogr. 26*, 282−291.

Blake, C. C. F., & Evans, P. R. (1974) *J. Mol. Biol. 84*, 585−601.

Blake, C. C. F., Evans, P. R., & Scopes, R. K. (1972) *Nature New Biol. 235*, 195−198.

Blake, C. C. F., & Rice, D. W. (1981) *Phil. Trans. R. Soc. Lond. A 293*, 93−104.

Brünger, A. T. (1992) *X-PLOR, Version 3.1, A system for X-ray crystallography and NMR*, Yale University Press, New Haven, CT.

Chothia, C., & Lesk, A. M. (1986) *EMBO J. 5*, 823−826.

Cini, R., Burla, M. C., Nunzi, A., Polidori, G. P., & Zanazzi, P. F. (1984) *J. Chem. Soc., Dalton Trans.* 2467−2476.

Davies, G. J., Gamblin, S. J., Littlechild, J. A., Dauter, Z., Wilson, K. S., & Watson, H. C. (1994) *Acta. Crystallogr. D50*, 202−209.

Davies, G. J., Gamblin, S. J., Littlechild, J. A., & Watson, H. C. (1993) *Proteins: Struct., Funct., Genet. 15*, 283−289.

Desmadril, M., Minard, P., Ballery, N., Gaillard-Miran, S., Hall, L., Yon, J. (1991) *Proteins: Struct., Funct., Genet. 10*, 315−324.

Fairbrother, W. J., Hall, L., Littlechild, J. A., Walker, P. A., Watson, H. C., & Williams, R. J. P. (1989a) *FEBS Lett. 258*, 247−250.

Fairbrother, W. J., Walker, P. A., Minard, P. A., Littlechild, J. A., Watson, H. C., & Williams, R. J. P. (1989b) *Eur. J. Biochem. 183*, 57−67.

Fairbrother, W. J., Graham, H. C., & Williams, R. J. P. (1990) *Eur. J. Biochem. 190*, 161−169.

Furey, W., & Swaminathan, S. (1990) in *Program and Abstracts: American Crystallographic Association Meeting* Series 2, Vol. 18, p 73.

Haran, G., Haas, E., Szpikowska, B. K., & Mas, M. T. (1992) *Proc. Natl. Acad. Sci. U.S.A. 89*, 11764−11768.

Harlos, K., Vas, M., & Blake, C. F. (1992) *Proteins: Struct., Funct., Genet. 12*, 133−144.

Howard, A. J., Gilliland, G. L., Finzel, B. C., Poulos, T. L., Ohlendorf, D. H., & Salemme, F. R. (1987) *J. Appl. Crystallogr. 20*, 383−387.

Jones, T. A. (1985) *Methods Enzymol. 115*, 157−171.

Kabsch, W. (1976) *Acta Crystallogr. A32*, 922−923.

Kraulis, P. J. (1991) *J. Appl. Crystallogr. 24*, 946−950.

Larsson-Raznikiewicz, M., & Arvidsson, L. (1971) *Eur. J. Biochem. 22*, 506−512.

Larsson-Raznikiewicz, M. (1970) *Eur. J. Biochem. 15*, 574−580.

Laskowski, R. A., McArthur, M. W., Moss, D. S., & Thornton, J. M. (1993) *J. Appl. Crytallogr. 26*, 282−291.

Mas, M. T., Bailey, J. M., & Resplandor, Z. E. (1988) *Biochemistry 27*, 1168−1172.

Mouawad, L., Desmadril, M., Perahia, D., Yon, J. M., & Brochon, J. C. (1990) *Biopolymers 30*, 1151−1160.

Pickover, C. A., McKay, D. B., Engelman, D. M., & Steitz, T. A. (1979) *J. Biol. Chem. 254*, 11323−11329.

Sabat, M., Cini, R., Haromy, T., & Sundaralingam, M. (1985) *Biochemistry 24*, 7827−7833.

Saraste, M., Sibbald, P. R., & Wittinghofer, A. (1990) *Trends Biochem. Sci. 15*, 430−434.

Schierbeck, B., & Larsson-Raznikiewicz, M. (1979) *Biochim. Biophys. Acta 568*, 195−204.

Schulz, G. E. (1992) *Curr. Opin. Struct. Biol. 2*, 61−67.

Scopes, R. K. (1978a) *Enzymes 8*, 335−351.

Scopes, R. K. (1978b) *Eur. J. Biochem. 85*, 503−516.

Sherman, M. A., Szpikowska, B. K., Dean, S. A., Mathiowetz, A. M., McQueen, N. L., & Mas, M. T. (1990) *J. Biol. Chem. 265*, 10659−10665.

Sherman, M. A., Dean, S. A., Mathiowetz, A. M., & Mas, M. T. (1991) *Protein Eng. 4*, 935−940.

Sherman, M. A., Fairbrother, W. J., & Mas, M. T. (1992) *Protein Sci. 1*, 1−9.

Tanswell, P., Westhead, E. W., & Williams, R. J. P. (1976) *Eur. J. Biochem. 63*, 249−262.

Timchenko, A. A., & Tsyuryupa, S. N. (1982) *Biophysics 27*, 1065−1069.

Walker, P. A., Littlechild, J. A., Hall, L., & Watson, H. C. (1989) *Eur. J. Biochem. 183*, 49−55.

Watson, H. C., Walker, N. P. C., Shaw, P. J., Bryant, T. N., Wendell, P. L., Fothergill, L. A., Perkins, R. E., Conroy, S. C., Dobson, M. J., Tuite, M. F., Kingsman, A. J., & Kingsman, S. M. (1982) *EMBO J. 1*, 1635−1640.

Tronrud, D. E., Ten Eyck, L. F., Matthews, B. W. (1987) *Acta Crystallogr. A 43*, 489−501.

Vonrhein, C., Schlauderer, G. J., & Schulz, G. Z. (1995) *Structure 3*, 483−490.

BI952500O